

Storage and retrieval of a microwave field in a spin ensemble

Y. Kubo,¹ I. Diniz,² A. Dewes,¹ V. Jacques,³ A. Dréau,³ J.-F. Roch,³ A. Auffeves,² D. Vion,¹ D. Esteve,¹ and P. Bertet¹

¹*Quantronics group, SPEC (CNRS URA 2464), IRAMIS, DSM, CEA-Saclay, FR-91191 Gif-sur-Yvette, France*

²*Institut Néel, CNRS, BP 166, FR-38042 Grenoble, France*

³*LPQM (CNRS UMR 8537), ENS de Cachan, FR-94235 Cachan, France*

(Received 14 September 2011; published 30 January 2012)

We report the storage and retrieval of a small microwave field from a superconducting resonator into collective excitations of a spin ensemble. The spins are nitrogen-vacancy centers in a diamond crystal. The storage time of the order of 30 ns is limited by inhomogeneous broadening of the spin ensemble.

DOI: [10.1103/PhysRevA.85.012333](https://doi.org/10.1103/PhysRevA.85.012333)

PACS number(s): 03.67.Lx, 42.50.Ct, 42.50.Pq, 85.25.Cp

I. INTRODUCTION

Superconducting qubits are promising candidates for quantum-information processing; however their coherence times [1] cannot yet compete with those of microscopic systems such as atoms [2], or electrons and nuclear spins [3]. Hybrid quantum circuit architectures have thus been proposed [4–9], in which microscopic systems would be used as quantum memory for superconducting qubits. Whereas the coupling of one individual atom or spin to a superconducting circuit is usually too weak, the coupling constant of an ensemble of N such systems is enhanced by \sqrt{N} , allowing to reach the strong coupling regime requested for quantum-information applications. Proposals for spin-ensemble-based hybrid quantum circuits often consist of a superconducting resonator used as a quantum bus between the ensemble and the superconducting qubit. On the experimental side [10–15], strong coupling between a spin ensemble and a superconducting resonator has up to now been demonstrated only spectroscopically. Here we report time-domain measurements of the coherent storage and retrieval of a classical microwave field [16] of about 500 photons from a superconducting resonator into collective excitations of a spin ensemble consisting of negatively charged nitrogen-vacancy centers in diamond (NV centers), an important step toward a spin-based hybrid quantum circuit architecture.

The experiment relies on the fact that the interaction between the electromagnetic field in the cavity mode and the spin ensemble involves only one collective spin variable, which behaves as a harmonic oscillator in the limit of low excitation energy [8]. This effective spin oscillator is magnetically coupled with a collective coupling constant g_{ens} to the superconducting resonator whose frequency can be tuned. When two such coupled harmonic oscillators are suddenly put into resonance, they coherently exchange energy with a period π/g_{ens} . We observe this dynamics by measuring the amplitude of the microwave field leaking out of the resonator after its interaction with the spins, which is found to oscillate as a function of the interaction time. This storage-retrieval cycle is, however, damped in a relatively short time, which as we show is limited by the inhomogeneous broadening of the NV center ensemble. Quantitative agreement with recent theoretical work [17,18] is obtained for a consistent set of data, covering spectroscopic as well as time-domain measurements.

II. DIAMOND SAMPLE AND MEASUREMENT SETUP

A sketch of our experimental sample and setup is shown in Fig. 1. The core of the experiment consists of an ensemble of $\sim 10^{12}$ NV centers in a diamond crystal, magnetically coupled to a superconducting resonator.

The diamond crystal is of the high-pressure high-temperature Ib type, with a nominal 100 ppm nitrogen concentration. It was irradiated with 2.5 MeV protons at a dose of $5 \times 10^{16} \text{ cm}^{-2}$ in order to create vacancies and subsequently annealed at 900 °C for 10 h to form negatively charged NV centers. The resulting NV concentration, $\rho = (1.2 \pm 0.3) \times 10^6 \text{ } \mu\text{m}^{-3}$, was measured by comparing the sample photoluminescence under a laser excitation at 532 nm to the photoluminescence of an individual center under the same conditions. This diamond is glued on top of the resonator with vacuum grease as discussed in Ref. [11]. A static magnetic field, $B_{\text{NV}} = 1.7 \text{ mT}$, is applied using an outer coil to the spins, parallel to the chip surface, along the [1,0,0] crystal axis within a few degrees [see Fig. 1(b)]. With this orientation, the four possible NV center crystalline orientations all make approximately the same angle $\theta \simeq 55^\circ$ with B_{NV} so that their resonance frequencies [see Fig. 1(c)] are approximately equal.

The resonator is a superconducting coplanar waveguide resonator, which was made frequency-tunable by including a four-SQUID array in its center conductor. Tuning of the resonator frequency $\omega_r(\Phi)$ is performed by changing the flux Φ through the SQUID loops [19], which can be done on a nanosecond timescale [20] as discussed in more detail below.

The chip is fitted in a microwave printed circuit board and mounted inside a copper box thermally anchored to the mixing chamber of a cryogen-free dilution cryostat at 40 mK. The sample box and outer coil are surrounded by two magnetic shieldings consisting of permalloy tape VC6025X (VacuumSchmelze) and a superconducting lead cylinder.

For time-domain experiments, we need to send fast current pulses to tune the resonator frequency and to measure the amplitude $A(t)$ of microwave pulses transmitted through the resonator using homodyne detection followed by sampling and averaging. A complete description of the measurement setup used is shown in Fig. 2. [Figure 2(a) shows the room temperature setup, and Fig. 2(b) the wiring inside the fridge]

The fast current pulse (with rise time $\sim 2 \text{ ns}$) is generated by an arbitrary function generator AFG3251 (Tektronix), reaches the sample through attenuators and filters at low temperature, and goes back to room temperature through the

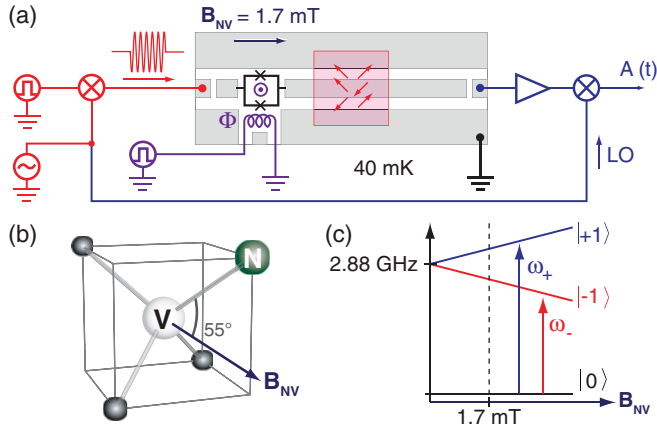


FIG. 1. (Color online) (a) Setup description. The NV center ensemble is magnetically coupled to the coplanar resonator containing a SQUID. The flux Φ through the SQUID loop can be tuned on a nanosecond scale by applying current pulses to an on-chip antenna. A magnetic field $B_{\text{NV}} = 1.7$ mT is applied to the spins, parallel to the sample and to the $[1,0,0]$ crystal axis (b). The amplitude $A(t)$ of microwave pulses transmitted through the resonator is measured by homodyne detection at room temperature after amplification. (c) Simplified energy level scheme of a NV center.

same combination of filters and attenuators. A close-up view of the flux line and SQUID array is shown in Fig. 3. Passing current through the on-chip antenna generates screening currents through the ground planes, as shown by the dashed arrows in Fig. 3(b), of our superconducting circuit with very low damping times (of the order of ns) that in turn affect the flux through the SQUIDs. As a result, the flux bias offset of the SQUIDs was found to depend on the time integral of the flux pulse. In addition, the flux applied to the SQUID loops by sending a fast current pulse through the flux line was strongly reduced (by a factor ~ 50) compared to the flux applied with a dc current of the same amount. We measure this current-to-flux transfer function with calibration experiments, allowing us to convert a voltage pulse into flux in the measurements described below. In order for the bias point to be independent of the amplitude and duration of the pulse, we had to add, at the end of each sequence, a compensation flux pulse opposite to the first one [see Fig. 3(c)]. Such a compensation pulse has strictly no incidence on the experiment outcome since it is applied long after the microwave signal is detected.

The microwave pulse is generated by mixing continuous microwave and a fast dc voltage pulse using an IQ mixer. The microwave pulse reaches the input port of the chip through a room-temperature tunable attenuator, low-temperature attenuators, and filters. The signal transmitted through the sample is amplified by a cryogenic HEMT amplifier with a noise temperature of ~ 4 K, further amplified at room temperature, demodulated into in (I) and quadrature (Q) phase components, and finally sampled at 500 MS/s by a data acquisition card Acqiris CC1065A (Agilent).

III. MEASUREMENTS AND DISCUSSION

We first characterize the resonator-spin system by measuring the resonator transmission $|S_{21}|(\omega)$ while scanning Φ . As shown in Fig. 4, two vacuum Rabi splittings are

observed when the resonator frequency matches either one of the two NV center transitions ω_- (resp. ω_+) from ground state $m_S = 0$ to $m_S = -1$ (resp. $m_S = +1$). A fit of these data using a coupled oscillators model [11] yields $g_{\text{ens}}/2\pi = 10.6$ MHz for the lower frequency anticrossing occurring at $\omega_-/2\pi = 2.85$ GHz, on which we focus in the following. The transmission close to the middle of the anticrossing is shown in Fig. 4 where two well-resolved polaritonic peaks can be seen, an indication that the two oscillators are in the strong coupling regime and that the coherent exchange of excitations between the resonator and the spin ensemble can be observed in the time domain.

To demonstrate such dynamics, the experiment proceeds as follows [see Fig. 5(a)]. At the beginning of each experimental sequence (averaged out typically 5×10^5 times), the resonator is biased at a flux Φ_{OFF} such that its frequency $\omega_r(\Phi_{\text{OFF}})/2\pi = 2.88$ GHz is out of resonance with the spins. A microwave pulse at frequency $\omega_r(\Phi_{\text{OFF}})$ of duration $2 \mu\text{s}$ (much longer than the resonator damping time $T_{\text{cav}} = Q/\omega_r \sim 100$ ns) establishes a steady-state coherent field of amplitude α inside the resonator (with $|\alpha|^2 \sim 500$ photons). Right after the microwave pulse is switched off ($t = 0$), the resonator frequency is brought close to ω_- by a flux pulse of amplitude $\Delta\Phi$ [see Fig. 4(a)] and duration τ , during which the resonator and the spin ensemble may exchange energy causing the intracavity field amplitude $|\alpha(t)|$ to oscillate. After the flux pulse, the only evolution of the field is an exponential decay $|\alpha(t > \tau)| = |\alpha(\tau)| \exp[-(t - \tau)/2T_{\text{cav}}]$. Measuring the amplitude of the exponentially damped microwave signal that leaks out of the cavity therefore directly yields $|\alpha(\tau)|$ and reveals the coupled resonator-spin dynamics.

Figure 5(b) shows the results obtained for a flux pulse amplitude $\Delta\Phi$ that puts the resonator in resonance with the spins at ω_- . The two-dimensional plot shows the measured microwave output amplitude $A(t)$ for increasing τ . The curve $A(t)$ for the shortest flux pulse $\tau = 5$ ns [see Fig. 5(c)] showing the microwave field decay after the pulse is switched off is only approximately exponential, due to a slight nonlinearity of the resonator caused by the presence of the SQUID [21], which we neglect in the following. For increasing τ , the curves $A(t)$ clearly display two parts: from $t = 0$ to $t = \tau$ rapid transient oscillations are observed, which are unfortunately difficult to quantitatively interpret due to the finite bandwidth of our homodyne detection setup. After $t = \tau$, $A(t)$ shows a decay similar to the one observed for the shortest pulse but with an amplitude that oscillates with τ with a period $T \sim 50$ ns, in quantitative agreement with the coupling strength estimated from the vacuum Rabi splitting $T \simeq \pi/g_{\text{ens}}$. This establishes that the observed oscillation is indeed due to cycles where the microwave field is first stored into a collective spin excitation ($0 < g_{\text{ens}}\tau < \pi$) and then retrieved ($\pi < g_{\text{ens}}\tau < 2\pi$). Curves corresponding to various steps of the cycle are also shown in Fig. 5(c). Note that by using a homodyne detection scheme we can only measure a field that has a well-defined phase relation with the local oscillator, implying that phase coherence is indeed preserved even after several (storage, retrieval) cycles. A full quantum state tomography would however be needed in order to assess the fidelity of the field storage at the quantum level, which is beyond the scope of the present work.

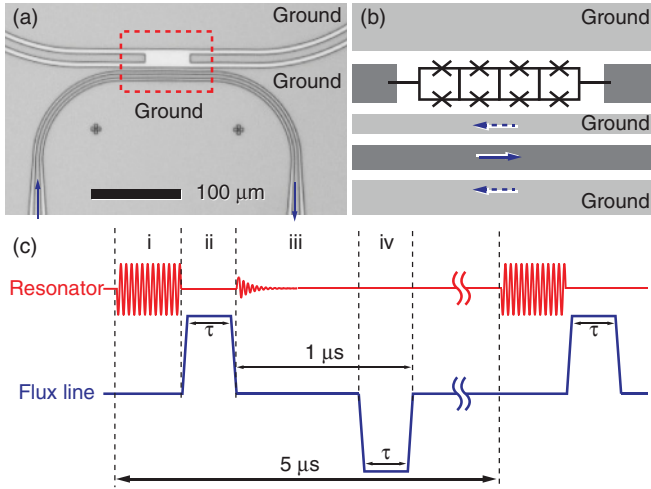


FIG. 3. (Color online) (a) Photograph of the area where the four-SQUID array is placed in the resonator (taken before fabrication of the SQUIDS). The arrows show the flow of an applied fast current pulse. (b) Close-up schematic of the SQUID array [dotted square in (a)]. The applied (return) current pulse is represented by a solid (dashed) arrow. (c) Actual pulse sequence for the measurement: (i) excitation, (ii) interaction, (iii) data accumulation, and (iv) compensation in the sequence. After data sampling (iii), an inverted pulse (iv) is applied to compensate the time integral to 0 (see text). The whole length of one sequence is 5 μ s.

broadening, an effect called *cavity protection* in Ref. [18]. In our experiment however we are not in the $g_{\text{ens}} \gg \Delta$ limit (see below) and these approximate formulas are not valid. We thus resort to an explicit analytical formula obtained using input-output relations on H [18], which allow us to calculate both the resonator transmission $t(\omega) = \kappa/[2i(\omega - \omega_r) - \kappa - 2iW(\omega)]$, with $W(\omega) = g_{\text{ens}}^2 \int_{-\infty}^{+\infty} \rho(\omega') d\omega'/[\omega - \omega']$ and $\kappa = \omega_r/Q$, and the time-domain signal as the modulus of the inverse Fourier-Laplace transform of $t(\omega)$ (see Ref. [18] and the Appendix).

To estimate these quantities in our experiment, we need to know the spin density distribution $\rho(\omega)$. In NV center

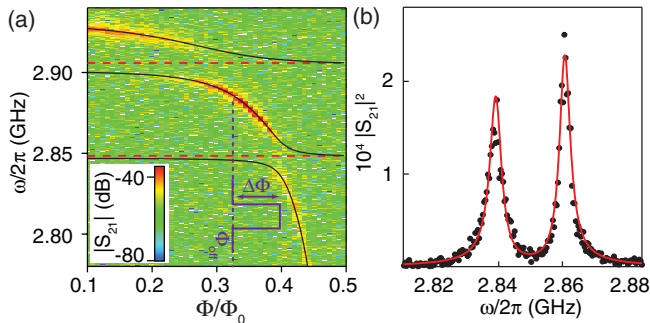


FIG. 4. (Color online) (a) Resonator transmission $|S_{21}|(\omega)$ at $B_{\text{NV}} = 1.7$ mT as a function of Φ (in units of the superconducting flux quantum $\Phi_0 = h/2e$) showing two vacuum Rabi splittings. The solid line is a fit to the data using the coupled oscillators model [11]. (b) Vacuum Rabi splitting close to resonance with ω_- . Black dots are experimental data; the red line is theory (rescaled in amplitude to fit the data) as explained in the text, assuming a spin-resonator detuning of 0.5 MHz.

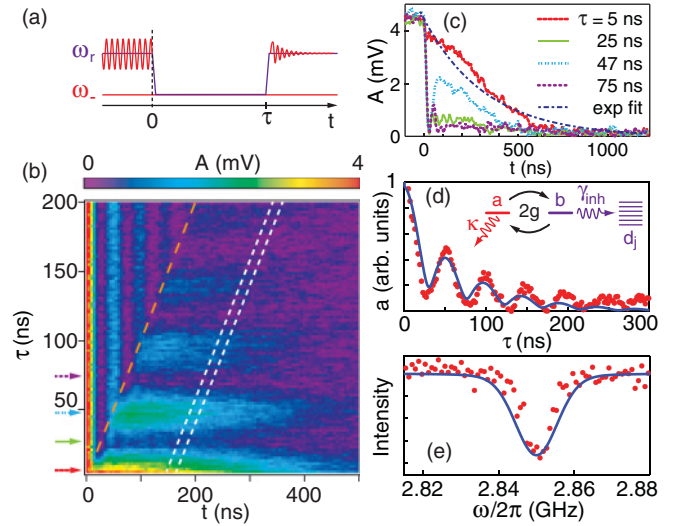


FIG. 5. (Color online) (a) Sketch of an experimental sequence. (b) Output amplitude $A(t)$ measured for increasing flux pulse duration τ , for a flux pulse amplitude such that $\omega_r(\Phi_{\text{OFF}} + \Delta\Phi) = \omega_-$. The long-dashed orange line indicates $t = \tau$. The two white dashed lines indicate the time window on which averaging is performed to compute $a(\tau)$ (see text). (c) Amplitude $A(t)$ for $g_{\text{ens}}\tau = 0, \pi, 2\pi, 3\pi$. (d) Normalized amplitude $a(\tau) = A(\tau + t_{\text{off}})$ (see text). Red dots are experimental data; the continuous blue line is theory as explained in the text. (Inset) Sketch of the physical process leading to damping of the oscillations because of coupling of the superradiant state to the bath of subradiant states. (e) Optically detected magnetic resonance signal measured at room temperature (red dots), compared to the spin distribution $\rho(\omega)$ (see text) used in the theoretical calculations (blue line).

ensembles, the inhomogeneous linewidth is caused by dipolar interactions with neighboring spins, either paramagnetic neutral single substitutional nitrogen (P1) impurities [22] that were not converted into NV centers during the sample processing or ^{13}C nuclei that are present in natural abundance (1.1%) [23]. Note that neighboring NV centers do not contribute to the inhomogeneous linewidth because at the temperature of our experiment they are frozen in the $m_S = 0$ state. In our sample, a FWHM linewidth $\Delta/2\pi \sim 7$ MHz was measured by optically detected magnetic resonance (ODMR) at room temperature [see Fig. 5(e)], compatible with the linewidth expected from its nominal P1 centers concentration of ~ 100 ppm [23]. As shown in Refs. [17,18], quantitative predictions for the system dynamics require one to know not only the overall linewidth but also the detailed shape of $\rho(\omega)$. In particular Gaussian and Lorentzian distributions yield very different results. Spin ensembles inhomogeneously broadened by dipolar interactions are expected to show a Lorentzian lineshape [24] with a cutoff. However, complications in our experiment arise due to hyperfine coupling with the ^{14}N atom nuclear spin, to a possible misalignment of B_{NV} with the [1,0,0] crystalline axis causing the four NV orientations to have slightly different frequencies, and to a possible spatial inhomogeneity of the NV centers' distribution originating from an inhomogeneous distribution of nitrogen in the diamond sample, often encountered in crystals grown by the high-pressure high-temperature method as is the case here [25]. As a result, we assume a phenomenological lineshape

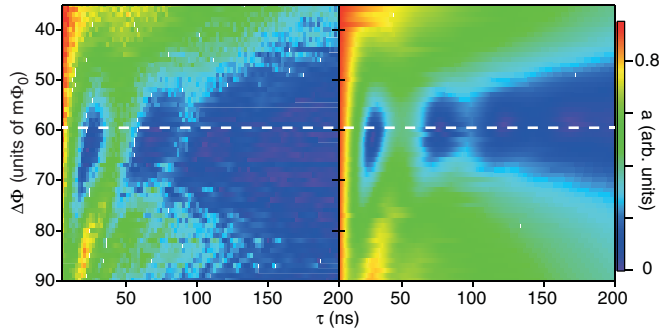


FIG. 6. (Color online) Coherent field exchange between the resonator and the spins for varying flux pulse amplitude $\Delta\Phi$. Normalized amplitude $a(\tau)$ (see text) is plotted versus τ and $\Delta\Phi$. The left graph is experimental data; the right graph is theory. The white dashed line indicates $\Delta\Phi$.

for our spin ensemble adjusted for reaching good agreement both with spectral and time-domain experimental data, as a convolution of a Gaussian and a Lorentzian profile with respective widths σ and γ (see the Appendix for more details). The parameters chosen in the following ($\sigma/2\pi = 5.12$ MHz and $\gamma/2\pi = 1$ MHz) yield a lineshape $\rho(\omega)$ compatible with ODMR data although slightly broader, as can be seen in Fig. 5(e). Using such a distribution and the formulas above, we obtain quantitative agreement for spectroscopic [see Fig. 4(b)] as well as time-domain [see Fig. 5(d)] measurements.

We also study the dependence of the microwave field exchange on the resonator-spin detuning by measuring $a(\tau)$ for various $\Delta\Phi$ (see Fig. 6). Out of resonance, the oscillations amplitude is reduced and their frequency increases as expected for two coupled oscillators. The asymmetry in the data between the $\Delta\Phi < \overline{\Delta\Phi}$ and $\Delta\Phi > \overline{\Delta\Phi}$ sides is an artifact of the nonlinear dependence of ω_r on $\Delta\Phi$ and of a residual hybridization of the resonator with the spins caused by the finite initial detuning [$\omega_r(\Phi_{\text{OFF}}) - \omega_-]/g \sim 3$, and is well reproduced by theory. The largest discrepancy is observed for pulse amplitudes $\Delta\Phi \sim 90 m\Phi_0$, where additional features are clearly seen in the experiment. We attribute them to a small density of NV centers having a ^{13}C among their closest neighbor, known to shift the electron spin frequency by ± 65 MHz due to the hyperfine interaction, and that was not taken into account in the calculation.

We finally perform a Ramsey-like experiment in order to quantify the time during which the microwave field can be stored in the spin ensemble. Starting as before with a steady-state microwave field in the resonator biased at Φ_{OFF} , the resonator is tuned in resonance with the spins at $t = 0$ for a $\pi/2$ pulse ($g_{\text{ens}}\tau = \pi/2$), after which it is detuned by $\Delta\omega/2\pi = 30$ MHz during Δt , then tuned back to resonance for a second $\pi/2$ pulse, and finally tuned back at $\omega_r(\Phi_{\text{OFF}})$, after which $a(\Delta t) = A(2\tau + \Delta t + t_{\text{off}})$ is measured. Due to the beating between the effective spin oscillator and the resonator, oscillations are observed in $a(\Delta t)$ at frequency $\Delta\omega$ as seen in Fig. 7. The oscillations amplitude decay time of ~ 30 ns gives the storage time, on the order of $\sim 2/\Delta$ as expected. The full calculation, performed as explained above, yields again reasonable agreement with the measurements.

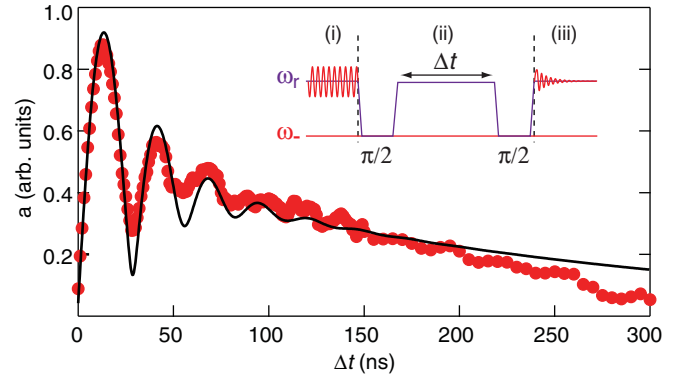


FIG. 7. (Color online) Ramsey fringes experiment. The normalized microwave amplitude $a(\Delta t)$ after the pulse sequence shown in the inset is plotted. Red dots are experimental data; the black continuous line is theory.

IV. PERSPECTIVES AND CONCLUSION

As shown by these results, inhomogeneous broadening appears as a serious obstacle to the successful implementation of hybrid quantum circuits based on spin ensembles. One first obvious solution is to obtain samples with narrower inhomogeneous linewidths. In the specific case of NV centers, this requires a very efficient conversion rate η of P1 centers initially present in the diamond crystal in NV centers. Improvement by 1 order of magnitude compared to the sample used in this work (where η is a few percent) is within reach. This would reduce the inhomogeneous linewidth by the same amount, at which point inhomogeneous broadening would be dominated by the NV centers' hyperfine structure ($\Delta/2\pi \sim 4$ MHz for ^{14}N). Another solution is to increase the NV concentration even further to reach the regime $g_{\text{ens}} \gg \Delta$ and rely on the cavity protection effect. Finally, it should be possible, by applying refocusing techniques used for atomic ensemble-based quantum memories [26], to recover the quantum information lost in the dark states into the superradiant state and then into the resonator. This would be the best way to fully benefit from the spin superior coherence properties.

Note added. Recently, two related experiments demonstrating the coherent storage and retrieval of a single excitation from a superconducting qubit have been reported [27,28].

ACKNOWLEDGMENTS

We gratefully thank P. Sénat, J.-C. Tack, P.-F. Orfila, M. de Combarieu, P. Forget, and P. Pari for technical help, and we acknowledge useful discussions within the Quantronics group. We acknowledge the support of the European Contracts MIDAS and SOLID.

APPENDIX

We now give more details on the theory calculations. All these calculations are performed in the Holstein-Primakoff approximation, in which the spins and the resonator are described by harmonic oscillators, as explained in the text.

The system Hamiltonian is $H/\hbar = \omega_r(\Phi)a^\dagger a + \sum \omega_j b_j^\dagger b_j + \sum i g_j (b_j^\dagger a - b_j a^\dagger)$, g_j being the coupling constant of spin j with the resonator.

1. Rabi oscillations

We first calculate the oscillating signal resulting from the cycles of storage and retrieval of the resonator field of amplitude α into the spin ensemble (Fig. 5). A first remark is that for the system consisting of coupled harmonic oscillators, its time evolution does not depend on the initial field amplitude. As a result we only calculate $\alpha_{\text{Rabi}} = \langle 0|a(t)a^\dagger(0)|0\rangle$, which represents the probability amplitude that a photon created at $t=0$ is still present at time t . As shown in Ref. [18] this quantity can be calculated by considering an effective non-Hermitian Hamiltonian

$$H_{\text{eff}}/\hbar = \begin{pmatrix} \tilde{\omega}_0 & i g_1 & i g_2 & \dots \\ -i g_1 & \tilde{\omega}_1 & & \\ -i g_2 & & \tilde{\omega}_2 & \\ \vdots & & & \ddots \end{pmatrix}, \quad (\text{A1})$$

with complex angular frequencies $\tilde{\omega}_0 = \omega_r - i\kappa/2$ and $\tilde{\omega}_k = \omega_k - i\gamma_0/2$; here, γ_0 is the spontaneous emission rate of each spin (that we take here to be zero since NV centers at low temperature have negligible energy relaxation). Indeed, introducing the vector $X(t)$ of coordinates $[\langle a(t)a^\dagger(0)\rangle, \dots, \langle b_j(t)a^\dagger(0)\rangle, \dots]$ it can be shown that $dX/dt = -(i/\hbar)H_{\text{eff}}X$. The formal solution to this equation is then

$$X(t) = \mathcal{L}^{-1}[(s + iH_{\text{eff}}/\hbar)^{-1}X(0)], \quad (\text{A2})$$

with $X(0) = x_G$ and $x_G \equiv (1, 0, \dots, 0)$. This implies that $\alpha(t) = x_G^\dagger X(t) = \mathcal{L}^{-1}[t_1(s)]$ with $t_1(s) = x_G^\dagger (s + iH_{\text{eff}})^{-1} x_G$ and $\mathcal{L}[f(s)] = \int e^{-st} f(t) dt$, s being a complex number. Since $t_1(s)$ is not singular on its imaginary axis, we only need t_1 for pure imaginary argument $s = -i\omega$ to perform the Laplace transform inversion. As shown in Ref. [18], we have $t_1(-i\omega) = i/[\omega - \omega_0 + i\kappa/2 - W(\omega)]$, with $W(\omega) = g_{\text{ens}}^2 \int \rho(\omega') d\omega' / [\omega - \omega' + i\gamma_0/2]$. Computing $\alpha(t)$ is thus achieved by evaluating t_1 for the distribution $\rho(\omega)$ described in the main text and numerically evaluating the inverse Laplace transform. This calculation also enables us to calculate the transmission as plotted in Fig. 4, because as shown in Ref. [18], the resonator transmission is obtained as $t(\omega) = -(\kappa/2)t_1(-i\omega)$.

An additional complication in the experiment is that the resonator-spin detuning δ during the microwave pulse is finite, implying that the initial state is actually already hybridized. To take this into account in the calculation, we make the approximation that this initial state is a coherent superposition of x_G and $x_S \equiv (0, g_1, \dots, g_j, \dots, g_N)/g_{\text{ens}}$. The vector x_S is associated with the excitation of the superradiant mode. Thus the initial state is written $x(t=0) = \cos(\theta/2)x_G + i \sin(\theta/2)x_S$, with mixing angle $\tan \theta = 2g_{\text{ens}}/\delta$. Using a similar analysis, we now have $\alpha_{\text{Rabi}} = \cos(\theta/2)\mathcal{L}^{-1}[t_1(s)] + i \sin(\theta/2)\mathcal{L}^{-1}[t_4(s)]$. In addition to $t_1(s)$ we then need $t_4(s) = x_G^\dagger (s + iH_{\text{eff}})^{-1} x_S$, as shown in Ref. [18], $t_4(-i\omega) = -it_1(-i\omega)W(\omega)/g_{\text{ens}}$.

2. Ramsey fringes

Each $\pi/2$ pulse necessary to realize the Ramsey-like experiment is realized by bringing the resonator and spins to resonance. For a fast pulse, the resonant interaction maps continuously the coherent state of the field to the superradiant mode in the spins. We calibrate the interaction time in such a way as to transform the state x_G into the superposition $\frac{x_G - x_S}{\sqrt{2}}$. After the first $\pi/2$ pulse, the resonator is kept detuned from the spin ensemble for a time t . The system state at this point can be evaluated using Eq. (A2). We define $X_G(t)$ [resp. $X_S(t)$] as the vector of coordinates $[\langle a(t)a^\dagger(0)\rangle, \dots, \langle b_j(t)a^\dagger(0)\rangle, \dots]$ at time t with initial conditions x_G (resp. x_S). A second $\pi/2$ pulse is then applied before the amplitude α_{RF} of the field in the resonator is measured:

$$\begin{aligned} \alpha_{\text{RF}} &= \frac{1}{\sqrt{2}} x_G^\dagger U_{\pi/2} [X_G(t) - X_S(t)] \\ &= \frac{1}{2} (x_G^\dagger + x_S^\dagger) [X_G(t) - X_S(t)] \\ &= \frac{1}{2} \mathcal{L}^{-1}[t_1(s) - t_2(s) + t_3(s) - t_4(s)], \end{aligned} \quad (\text{A3})$$

where $t_2(s) = x_S^\dagger (s + iH_{\text{eff}})^{-1} x_S$ and $t_2(s) = x_S^\dagger (s + iH_{\text{eff}})^{-1} x_G$, and t_1 and t_4 are defined above. As shown in Ref. [18], $t_2(-i\omega) = -t_1(-i\omega)W(\omega)(s + i\tilde{\omega}_0)/g_{\text{ens}}^2$ and $t_3 = -t_4$.

3. Density distribution

The spin density distribution that we use is the convolution of a normalized Gaussian of standard deviation σ with a normalized Lorentzian of HWHM γ . The resulting distribution is known as the Voigt profile and is also normalized:

$$\begin{aligned} \rho(\omega'; \sigma, \gamma) &= \int_{-\infty}^{\infty} G(\omega''; \sigma) L(\omega' - \omega''; \gamma) d\omega'' \\ &= \frac{1}{\sigma\sqrt{2\pi}} \frac{\gamma}{\pi} \int_{-\infty}^{\infty} \frac{e^{\omega''^2/2\sigma^2}}{(\omega' - \omega'')^2 + \gamma^2} d\omega''. \end{aligned} \quad (\text{A4})$$

An important property is that we can compute analytically the function $W(\omega)$:

$$\begin{aligned} W(\omega; \sigma, \gamma, \gamma_0) &= \frac{\Omega^2}{\sigma\sqrt{2\pi}} \frac{\gamma}{\pi} \int \int \frac{e^{\omega''^2/2\sigma^2}}{(\omega' - \omega'')^2 + \gamma^2} \\ &\quad \times \frac{d\omega' d\omega''}{\omega - \omega' + i\gamma_0}. \end{aligned} \quad (\text{A5})$$

Taking the limit $\gamma_0 \rightarrow 0$, we have

$$\begin{aligned} W(\omega; \sigma, \gamma) &= -i\sqrt{\frac{\pi}{2}} \frac{\Omega^2}{\sigma} \exp\left\{-\left(\frac{\omega + i\gamma}{\sigma\sqrt{2}}\right)^2\right\} \\ &\quad \times \text{erfc}\left(-i\frac{\omega + i\gamma}{\sigma\sqrt{2}}\right). \end{aligned} \quad (\text{A6})$$

The function that is taken in the theory actually takes into account the well-known NV center hyperfine splitting due to ^{14}N by adding up three identical distributions $\rho(\omega)$ separated by 2.2 MHz [29]. The resulting distribution is the one shown in Fig. 5. This is conveniently done since $W[\rho_1 + \rho_2] = W[\rho_1] + W[\rho_2]$ for any two different spin distributions $\rho_{1,2}$. Using this formula for $W(\omega)$ we can evaluate the functions t_i necessary for the simulation of the Rabi and Ramsey-like experiments.

- [1] H. Paik *et al.*, *Phys. Rev. Lett.* **107**, 240501 (2011).
- [2] C. F. Roos, G. P. T. Lancaster, M. Riebe, H. Haffner, W. Hansel, S. Gulde, C. Becher, J. Eschner, F. Schmidt-Kaler, and R. Blatt, *Phys. Rev. Lett.* **92**, 220402 (2004).
- [3] G. Balasubramanian *et al.*, *Nat. Mater.* **8**, 383 (2009).
- [4] P. Rabl, D. DeMille, J. M. Doyle, M. D. Lukin, R. J. Schoelkopf, and P. Zoller, *Phys. Rev. Lett.* **97**, 033003 (2006).
- [5] D. Petrosyan, G. Bensky, G. Kurizki, I. Mazets, J. Majer, and J. Schmiedmayer, *Phys. Rev. A* **79**, 040304(R) (2009).
- [6] J. Verdu, H. Zoubi, C. Koller, J. Majer, H. Ritsch, and J. Schmiedmayer, *Phys. Rev. Lett.* **103**, 043603 (2009).
- [7] A. Imamoglu, *Phys. Rev. Lett.* **102**, 083602 (2009).
- [8] J. H. Wesenberg, A. Ardavan, G. A. D. Briggs, J. J. L. Morton, R. J. Schoelkopf, D. I. Schuster, and K. Molmer, *Phys. Rev. Lett.* **103**, 070502 (2009).
- [9] D. Marcos, M. Wubs, J. M. Taylor, R. Aguado, M. D. Lukin, and A. S. Sorensen, *Phys. Rev. Lett.* **105**, 210501 (2010).
- [10] I. Chiorescu, N. Groll, S. Bertaina, T. Mori, and S. Myiashita, *Phys. Rev. B* **82**, 024413 (2010).
- [11] Y. Kubo *et al.*, *Phys. Rev. Lett.* **105**, 140502 (2010).
- [12] D. I. Schuster *et al.*, *Phys. Rev. Lett.* **105**, 140501 (2010).
- [13] R. Amsuss *et al.*, *Phys. Rev. Lett.* **107**, 060502 (2011).
- [14] P. Bushev, A. K. Feofanov, H. Rotzinger, I. Protopopov, J. H. Cole, C. M. Wilson, G. Fischer, A. Lukashenko, and A. V. Ustinov, *Phys. Rev. B* **84**, 060501 (2011).
- [15] E. Abe, H. Wu, A. Ardavan, and J. J. L. Morton, *Appl. Phys. Lett.* **98**, 251108 (2011).
- [16] H. Wu, R. E. George, J. H. Wesenberg, K. Molmer, D. I. Schuster, R. J. Schoelkopf, K. M. Itoh, A. Ardavan, J. J. L. Morton, and G. A. Briggs, *Phys. Rev. Lett.* **105**, 140503 (2010).
- [17] Z. Kurucz, J. H. Wesenberg, and K. Molmer, *Phys. Rev. A* **83**, 053852 (2011).
- [18] I. Diniz, S. Portolan, R. Ferreira, J. M. Gerard, P. Bertet, and A. Auffeves, *Phys. Rev. A* **84**, 063810 (2011).
- [19] A. Palacios-Laloy, F. Nguyen, F. Mallet, P. Bertet, D. Vion, and D. Esteve, *J. Low Temp. Phys.* **151**, 1034 (2008).
- [20] M. Sandberg, C. M. Wilson, F. Persson, T. Bauch, G. Johansson, V. Shumeiko, T. Duty, and P. Delsing, *Appl. Phys. Lett.* **92**, 203501 (2008).
- [21] F. R. Ong, M. Boissonneault, F. Mallet, A. Palacios-Laloy, A. Dewes, A. C. Doherty, A. Blais, P. Bertet, D. Vion, and D. Esteve, *Phys. Rev. Lett.* **106**, 167002 (2011).
- [22] A. Cox, M. E. Newton, and J. M. Baker, *J. Phys. Condens. Matter* **6**, 551 (1994).
- [23] J. A. van Wyk, E. C. Reynhardt, G. L. High, and I. Kiflawi, *J. Phys. D* **30**, 1790 (1997).
- [24] V. V. Dobrovitski, A. E. Feiguin, D. D. Awschalom, and R. Hanson, *Phys. Rev. B* **77**, 245212 (2008).
- [25] R. C. Burns, V. Cvetkovic, C. N. Dodge, D. J. F. Evans, M.-L. T. Rooney, P. M. Spear, and C. M. Welbourn, *J. Cryst. Growth* **104**, 257 (1990).
- [26] A. I. Lvovsky, B. C. Sanders, and W. Tittel, *Nat. Photonics* **3**, 706 (2009).
- [27] Y. Kubo *et al.*, *Phys. Rev. Lett.* **107**, 220501 (2011).
- [28] X. Zhu *et al.*, *Nature (London)* **478**, 221 (2011).
- [29] V. Acosta *et al.*, *Phys. Rev. B* **80**, 115202 (2009).